CATO-2 Deliverable WP3.03-D04

Laboratory facilities for transport and mechanical properties determination (1st Year Progress Report)

Prepared by: Jon Samuelson
Bart Verberne
Karl-Heinz Wolff
Mariëlle Koenen
Tjirk Benedictus
Jan ter Heege
Tim Tambach

Reviewed by: C.J. Spiers

Approved by: J.Brouwer
(CATO-2 Director)

1 Executive Summary (restricted)

In WP 3.03, a wide array of experimental facilities will be brought to bear on the task of investigating the transport and mechanical properties of the caprock in CO_2 sequestration reservoirs. The present work is divided into separate sections describing apparatus and methodological developments from three different laboratories.

1) Utrecht University – HPT Laboratory
   a. Triaxial Deformation Apparatus (Heard)
      i. Triaxial Compressive Failure
         1. To develop a failure envelope for CO_2 reservoir caprock and determine how mechanical strength is affected by supercritical CO_2 which could lead to failure of the caprock and loss of reservoir integrity
      ii. Direct Shear Friction
         1. To measure the coefficient of friction of caprock derived fault gouge and determine how supercritical CO_2 pore fluid can alter frictional strength. Significant changes could result in fault reactivation
         2. To measure the frictional stability of caprock derived fault gouge and determine how supercritical CO_2 pore fluid can alter frictional stability. Significant changes could result in increased seismicity.
      iii. Fault Zone Permeability
         1. Measurement of the permeability of simulated fault zones to determine the degree to which ongoing reaction with supercritical CO_2 may alter the sealing ability of laterally bounding fault zones
   b. Argon Permeameter (APE)
      i. Low Confining Pressure (≤ 2 MPa)
         1. Argon Transient Step (ATS) permeability measurements on Röt and Solling caprock to investigate variations in permeability based on mineralogy, orientation to bedding, formation of origin, etc.
         2. Argon Flow Through permeability tests will be used to validate the findings of the more precise ATS method
      ii. High confining pressure (≤ 100 MPa) measurements of permeability will be conducted to determine if there is a significant systematic variation in permeability based on confining pressure.
   c. Autoclave and cold-seal reaction vessels will be used to analyze the long term mineralogical changes likely in caprock and caprock derived fault gouge under CO_2 reservoir conditions, and also to provide large volumes of reacted caprock gouge for use in frictional experiments.

2) TNO-Rijswijk – Prins Maurits Laboratory
   a. Static batch reaction vessel which will allow for long term reaction experiments on cylindrical caprock samples under CO_2 reservoir conditions with very limited ability for extensive fluid flow and also under more dynamic conditions to analyze the effects of pore fluid mobility on the degradation of caprock.

3) Technical University Delft – Laboratory of Geotechnology
   a. Large sample triaxial tresting machines - use of ductile metal sample jackets capable of withstanding the aggressive conditions associated with investigating chemical

interactions in the caprock-fracture-CO_2-H_20 system, such as fracture compaction, dissolution, (re-)mineralization, and permittivity.

Distribution List

(this section shows the initial distribution list)

External	Copies	Internal	Copies

Document Change Record

(this section shows the historical versions, with a short description of the updates)

Version	Nr of pages	Short description of change	Pages

Table of Contents

2 Applicable/Reference documents and Abbreviations

Applicable Documents

(Applicable Documents, including their version, are documents that are the "legal" basis to the work performed)

	Title	Doc nr	Version date
AD-01	Beschikking (Subsidieverlening CATO-2 programma verplichtingnummer 1-6843	ET/ED/9078040	2009.07.09
AD-02	Consortium Agreement	CATO-2-CA	2009.09.07
AD-03	Program Plan	CATO2-WP0.A-D.03	2009.09.29

Reference Documents

(Reference Documents are referred to in the document)

	Title	Doc nr	Version/issue	Date

Abbreviations

(this refers to abbreviations used in this document)

3 General Text

INTRODUCTION:

What follows is a three-part progress report of the experimental capabilities of the Utrecht University HPT Laboratory, the TNO-Rijswijk Prins Maurits Laboratory, and the Laboratory of Geotechnology at Delft University of Technology.

1) The Utrecht University HPT Laboratory has a wide variety of machines, largely focused on mechanical deformation and permeability analysis, as well as reaction vessels which will be used to simulate the environment of a CO_2 sequestration reservoir to investigate changes in the permeability and mechanical properties of caprock and fault gouge.
2) The TNO-Rijswijk Prins Maurits Laboratory is developing a new apparatus in which they will conduct static reaction experiments between CO_2-rich brine and caprock, cement, and formation rocks.
3) The Laboratory of Geotechnology at Delft University of Technology will conduct experiments aimed at measuring poroelastic interaction between the fluid (CO_2, brine, hydrocarbon) and the caprock using a lead-foil barrier to isolate confining fluid from the experimental rock sample.

UTRECHT UNIVERSITY HPT LABORATORY - EXPERIMENTAL METHODS:

Heard tri-axial pressure cell:

The majority of experiments conducted to answer the questions posed in Work Package 3.3 – Deliverable 08 will be performed in the Heard vessel, a constant confining volume tri-axial pressure vessel, capable of generating 100 MPa of confining pressure, using a silicone based oil, at temperatures in excess of 250 °C (Figures 1 & 2). The upper limit of experimental temperature is limited in the case of this experimental

analysis mainly by the jacketing material used to isolate pore fluid from the confining oil. The Heard vessel is an extremely versatile apparatus, capable of unconfined compressive strength, tri-axial compressive strength, saw cut friction, direct-shear friction, permeability, electrical impedance, hydrofracture experiments, and more [Peach, 1991; Peach and Spiers, 1996; Watanabe and Peach, 2002; Hangx, 2009; Hangx et al., 2009; Hangx et al., 2010; Hangx et al., 2010b; Liteanu, 2009; Liteanu, et al., 2009].

Cylindrical experimental samples (whether direct shear, saw cut, or rock core) are fitted between two pistons shown in Figure 1B and schematically in Figure 2, and jacketed using fluorinated ethylene propylene (FEP) in the case of compressive strength experiments, or ethylene propylene diene Monomer (EPDM) in the case of shear experiments. The experimental sample is then affixed to the vessel headpiece, inverted, and slid into the top of the pressure vessel. Once the pressure vessel is sealed a small (~ 3 MPa) amount of pressure is applied to the sample and the vessel is brought to experimental temperature using the external furnace (Figures 1A & 2). As the confining oil undergoes thermal expansion confining pressure builds up in the vessel and is periodically bled off to ensure that it remains beneath the intended experimental pressure. Once experimental temperature is reached, the vessel is brought to its final pressure and allowed to equilibrate for approximately 1 hour. When the Heard vessel has reached pressure and temperature equilibrium the experimental sample is loaded axially from underneath at a constant velocity, though velocity will be varied systematically in shearing experiments in order to determine the frictional stability of fault gouges in the reservoir system. Axial loading rates in the Heard apparatus can be varied over a 1000-fold range, from nearly plate rate velocities (~0.05 μm/s) up to velocities encroaching the nucleation rate for earthquakes (50 μm/s).

Tri-axial compressive strength:

The tri-axial compressive strength of caprock samples 13, and 53-60 will be measured at in-situ temperature (~115 °C) over a range of effective pressures (confining

pressure – pore fluid pressure) from 1.5 to 50 MPa, in a similar manner to experiments conducted by *Hangx et al.* [2010] and *Liteanu et al.* [2009]. Of the seven samples available for compressive strength measurements four will be analyzed under dry conditions, and the remaining three will be saturated with formation water (2M NaCl, 0.2M $CaCl_2$, 0.04M $MgCl_2$) and pressurized internally with supercritical CO_2. The goal of these experiments will be to produce a failure envelope for materials similar to the caprock in the P18 gas field and also to see how the strength of the caprock will be affected by reaction with CO_2 and brine under conditions similar to what will be present in the reservoir during the period of CO_2 sequestration.

Samples 53-60 are cores drilled parallel to bedding, and it is very possible that this may have an influence on the compressive strength values we measure in the Heard apparatus. We therefore hope to compare the measurements of cores 53-60 to that of core 13, which is cored perpendicular to bedding. If there is a strong variation in strength of the caprock based on the orientation of the core to bedding, it may necessitate additional sampling at the NAM core repository in order to provide a robust analysis of caprock strength both parallel and perpendicular to bedding.

Frictional strength and stability:

In order to determine whether the frictional strength and/or stability of cap-rock-derived fault gouge will be affected by the presence of sequestered CO_2 we have planned a series of direct shear experiments to be conducted in the Heard apparatus. The geometry of these experiments (Figure 1C & 1D) is a unique design dubbed “inverted-shear” due to the inversion of two identical forcing blocks. This geometry will allow us to conduct experiments which will have modestly high shear strain values (~7 on a 1 mm thick gouge layer) while avoiding the troublesome reality of constantly changing normal stress inherent in so-called “saw cut” friction experiments because at all times the normal stress on the gouge layer will be equal to the confining pressure. The inverted-shear experiments will be conducted by spreading a thin (~ 1 mm) layer of powdered caprock

on one of the blocks, and sandwiching the gouge layer with the inverted second block (Figure 1D). The void space between the ends of the two forcing blocks represents the major challenge of this geometry of direct-shear, though the current solution of filling the gaps with plugs of indium metal is sufficient for measuring shear strength, if not stability. The block-gouge sandwich is fitted between the top and bottom piston as shown in Figures 1B and 2, affixed to the headpiece, and slid into the Heard apparatus in the same fashion as for a compressive failure experiment.

Frictional strength will be measured by applying a confining pressure to the inverted-shear blocks, compressing the gouge layer between them. The loading yoke of the Heard apparatus is then driven up at a constant velocity until it comes into contact with the sample and begins transmitting load to the inverted-shear assembly and shearing the gouge layer. We monitor confining pressure, axial force, and displacement of the yoke constantly throughout the duration of the experiment. In the case of a granular material, for which cohesion is presumed to be zero, the coefficient of friction (μ) is the ratio of shear stress (τ) over effective normal stress (σ')

$$\mu = \frac{\tau}{\sigma'} \qquad (1)$$

Shear stress is the axial load normalized by the contact area (A) of the gouge layer (35 x 50 mm) and σ' is the confining pressure minus any pore fluid pressure.

Measurement of the coefficient of friction for the gouge material present in reservoir and caprock fault zones is important because, as mentioned previously, changes in the stress state of the fault zones as a function of withdrawing hydrocarbons or injecting CO_2 is known to cause fault reactivation and seismicity. In the case of Carbon Capture and Storage the CO_2 pore fluid will react with the bounding fault gouge over the long time scale of sequestration and perhaps alter the strength of the fault resulting in reactivation and seismicity even in cases where alterations to the stress state of the reservoir are minimal. We will measure μ for both dry caprock gouge and also for gouge

saturated with formation water and pressurized with super critical CO_2 in order to determine the first-order affect of CO_2 sequestration of fault zone strength.

Over the short time duration of any individual shearing experiment (< 72 hours) it is difficult to imagine that mineralogical changes in the gouge layer will be significant, even at in-situ pressure and temperature conditions (35 MPa, 115 °C). The most likely influence of supercritical CO_2 on frictional strength on this time scale is that the CO_2 will desiccate the clay minerals in the powdered caprock. Previous experiments have shown, with certain clay minerals, that increased hydration state can result in decreased frictional strength [*Ikari et al.*, 2007], this suggests that CO_2 acting to dry out the clay minerals in the caprock gouge could result in increased frictional strength and reduced likelihood of fault reactivation and seismicity.

In addition to the short term influence of CO_2 on friction by dehydrating clay minerals, it is exceedingly important to understand the longer term mineralogical changes that may result in alterations in frictional strength and stability. We will use a 1-liter autoclave reaction vessel to subject large volumes of powdered caprock to 30 MPa of CO_2 pressure at ~ 100 °C (discussed more thoroughly below). We will periodically harvest enough of the gouge powder to conduct an inverted-shear experiment in the Heard vessel, and also to analyze the mineralogical changes to the powder. Given sufficient sample quantity we will be able to harvest reacted caprock every 4-6 weeks for at least 1 year, which will provide an ideal opportunity to measure the long term effects of CO_2 sequestration on the strength and stability of reservoir and caprock faults.

Permeability:

One of the main concerns about CCS is the possibility of CO_2 leaking out of the reservoir through the bounding fault zones. It is reasonable to assume that the faults currently act as an efficient barrier to fluid flow due to their having prevented the escape of gas for millions of years. There is however no certainty that reaction with CO_2 under

sequestration conditions will not change the structure and mineralogy of the fault zones in such a way that permeability is significantly increased and integrity is compromised.

In order to measure the fault perpendicular permeability of gouges in the Heard apparatus the inverted-shear blocks have been fitted with sintered stainless steel fluid distribution frits allowing for pore fluid (water or Argon gas) to be evenly distributed over the surface of the gouge layer, and provided a pressure imbalance across the layer, measurements of permeability. By connecting the pore fluid inlets of the Heard apparatus (Figure 3) to an Argon gas permeameter (discussed below) we will measure the permeability of caprock fault gouge pre- and post-shearing, providing us with an indication of the effect of shear strain on fault gouge permeability. We will also be able to analyze the longer term effects of changing mineralogy due to continued reaction with CO_2 by measuring the permeability of those gouge samples which have been aged in an autoclave for longer durations.

Argon gas permeameter:

Knowing the permeability of the reservoir caprock and bounding fault zones, and how the permeability of these features can change over the course of time when subjected to the corrosive conditions present in a CO_2 reservoir is one of the most fundamental questions regarding the CATO-2 project.

Using an Argon gas permeameter (APE) (Figure 3A) we have the ability to measure the permeability of cylindrical rock samples at low- and high-pressure conditions using two different methods. Using a small pressure vessel (labeled “LP” in Figure 3A) we can subject cylindrical samples to a confining pressure of up to 3.5 MPa, and using a larger pressure vessel (labeled “HP” in Figure 3A) samples can be confined at pressures up to 100 MPa, both at room temperature. The LP-vessel is limited to samples 25 mm in diameter with length up to ~ 70 mm, and while the HP-vessel is currently set up for similarly sized samples, it could quickly be modified to accept much larger cores.

Using the APE we are able to conduct two very different types of permeability analysis, which allows us a simple method of validating any measurements we make. The Argon-transient-step method (ATS) will be used most commonly in our analyses, and the values measured by ATS will be confirmed using the Argon-flow-through (AFT) method.

In both the ATS and AFT techniques the sample is placed between two end pieces (Figure 3B) which are grooved to ensure even distribution of the argon gas over the ends of the sample, and jacketed using a bicycle inner-tube (BIT) so that gas flows only along the axis of the cylindrical sample. The jacketed sample is then placed inside of the LP- or HP-vessel and a hydrostatic confining pressure is applied, sealing the edges of the sample ensuring that flow occurs only along the length of the core. Because the pressures that the samples are subjected to are hydrostatic the HP-vessel is capable of approximating in-situ stress conditions. The permeability of most samples will be measured in the LP-vessel using 2 MPa confining pressure, a few select samples will be run in the HP-vessel and if significant systematic variations in permeability are detected as a function of confining pressure we will measure all samples in both the LP- and HP-vessels.

In the Argon-transient step method the sample is confined with 2 MPa confining pressure and then pressurized internally with ~ 1.6 MPa of Argon fluid pressure. Once the internal pore fluid pressure of the sample has equilibrated, a portion of the steel tubing of the APE is isolated from the sample, and reduced in pressure to ~ 1.4 MPa. The isolated low pressure portion of the APE tubing is then opened to the sample creating an instantaneous pressure transient across its length. By measuring the decay of the pressure imbalance between the upstream and downstream ends of the sample as they equilibrate towards a mean pressure of ~ 1.5 MPa, we are able to calculate the permeability (Figure 4). In order to correct for the Klinkenberg Effect we will also measure permeability at mean Argon pressures of 1.0 and 0.5 MPa (1.1 upstream/0.9 downstream & 0.6 upstream/0.4 downstream respectively) for very impermeable samples. Though current limitations in the ATS method prevent us from measuring permeability

less than approximately 10^{-19} m^2, we hope to soon be able to measure permeability down to 10^{-21} m^2.

In addition to the ATS method we will use an Argon-flow-through (AFT) method of determining the permeability of our samples in order to validate the measurements made using the transient-step method. The AFT method is nominally a constant head permeability test, using Argon as the pore fluid. As with the ATS method the sample is loaded into either the LP- or HP-vessel and confining pressure is applied. The upstream side of the sample is attached to a large Argon gas reservoir, which is effectively infinite in volume compared to the pore volume of the sample. The downstream end of the sample is connected to a capillary tube at atmospheric pressure. When the upstream end is pressurized Argon gas will flow through the sample, and the volume of expelled gas is measured in the capillary tube. After a simple correction for the expansion of the Argon gas at atmospheric pressure the volume of expelled gas can be used in Darcy's Law to calculate the permeability of the sample and verify the findings of the more precise ATS method.

Autoclave & cold seal reaction vessels:

The time scale of any individual compressive or frictional strength test is typically on the order of hours to perhaps days. Over this time scale it is unlikely that complete or even significant mineralogical changes occur within an experimental sample subjected to reservoir CO_2 conditions, be it rock core or gouge layer. In order to understand the mineralogical changes in caprock and gouge likely to result from CO_2 sequestration, and the effect those changes have on mechanical strength and stability, we will be using several instruments available in the Utrecht University HPT lab to simulate the environment of a CO_2 reservoir.

Because each inverted-shear experiment will consume approximately 1.75 cm^3 (50 x 35 x 1 mm) of gouge material we have developed a method of subjecting a large volume of gouge to supercritical CO_2 over a considerable length of time. Using a 1-liter

stainless steel autoclave fitted with an internal Teflon sleeve, we will react powdered volumes of caprock samples 12-14 at near CO_2 reservoir conditions (30 MPa, ~100 °C) in a stack of 30 cm^3 Teflon pots (Figure 5). To mimic the natural conditions of the reservoir we will include a small volume (~ 30 mL) of brine, similar in composition to the formation water present in the reservoir (2M NaCl, 0.2M $CaCl_2$, 0.04M $MgCl_2$ [*Bert de Wijn*, personal communication]), in the bottom well of the autoclave. We will harvest gouge material from the autoclave vessel approximately every 4-6 weeks over the course of 1 year in order to measure the progress of the reaction and ascertain the effects of long term CO_2 exposure on frictional strength and stability. Given the volume necessary to conduct an inverted-shear experiment we hope to be able to perform 8 or more experiments on each caprock gouge sample.

While the autoclave experiment will be the predominant method of measuring the ongoing consequence of CO_2 sequestration on the mineralogy of caprock, we will also be conducting additional tests under the auspices of Work Package 3.4 that will be of interest to WP3.3. A shortcoming of our autoclave technique for performing CO_2-caprock-brine reactions is that there is no way to ensure that the reaction products of one of the sample pots will not influence the reactions in the other pots by way of dissolved transport through the wet supercritical CO_2. To investigate the reactivity of the caprock at CO_2 reservoir conditions in a more tightly controlled environment we will conduct batch reaction experiments on powdered caprock samples at in-situ pressure temperature conditions (115 °C, 35 MPa), similar to those conducted by *Hangx and Spiers* [2009] investigating the reaction of feldspar with CO_2. In this type of experiment a very small (~ 0.1 g) amount of caprock will be powdered and placed in a Teflon lined reaction vessel (Figure 6) along with a small volume of formation water. The reaction vessel is then fitted inside of a cold seal pressure vessel and attached to a pressurized source of CO_2 and brought to experimental pressure. A furnace is lowered over the pressure vessel and the sample is brought to experimental temperature. Though this type of experiment provides far better control on the reactive environment than the autoclave experiments it

will not produce a sufficient volume of reacted caprock to use in inverted-shear experiments, thus the need for both techniques.

Acknowledgements:

The UU team would like to acknowledge TNO Bouw & Ondergrond in Utrecht, the TNO core repository in Zeist, and the NAM core repository in Assen for their assistance in obtaining the relevant core material. We would also like to thank Peter van Krieken, Gert Kastelein, and Eimert de Graaf for their assistance in designing maintaining laboratory facilities and performing laboratory experiments.

Bibliography:

Hangx, S. J. T. (2009), Geological storage of CO_2: Mechanical and chemical effects on host and seal formations, Utrecht University – Ph.D. Thesis, *Geologica Ultraiectina*, *311*, 213 pp.

Hangx, S. J. T., and C. J. Spiers (2009), Reaction of plagioclase feldspars with CO_2 under hydrothermal conditions, *Chemical Geology*, *265*, 89-98, doi: 10.1016/j.chemgeo.2008.12.005.

Hangx, S. J. T., C. J. Spiers, and C. J. Peach (2009), The mechanical behavior of anhydrite and the effect of CO_2 injection, *Energy Procedia*, *1*, 3485-3592.

Hangx, S. J. T., C. J. Spiers, and C. J. Peach (2010), Mechanical behavior of anhydrite caprock and implications for CO_2 sealing capacity, *Journal of Geophysical Research*, *115*(B7), doi: 10.1029/2009JB006954.

Ikari, M. J., D. M. Saffer, and C. Marone (2007), Effect of hydration state on the frictional properties of montmorillonite-based fault gouge, *Journal of Geophysical Research*, *112*, doi: 10.1029/2006JB004748.

Liteanu, E. (2009), Subsurface Impact of CO_2: Response of carbonate rocks and wellbore cement to supercritical CO2 injection and long-term storage, Utrecht University – Ph.D. Thesis, *Geologica Ultraiectina*, *310*, 184 pp.

Liteanu, E., C. J. Spiers, and C. J. Peach (2009), Failure behaviour wellbore cement in the presence of water and supercritical CO2, Energy Procedia, 1, 3553-3560, doi: 10.1016/j.egypro.2009.02.149

Peach, C. J. (1991), Influence of deformation on the fluid transport of salt rocks, Utrecht University Ph.D. Thesis, *Geologica Ultraiectina, 77*, 238 pp.

Peach, C. J., and C. J. Spiers (1996), Influence of crystal plastic deformation on dilatancy and permeability development in synthetic salt rock, *Tectonophysics*, *256*, 101-128.

Watanabe, T., and C. J. Peach (2002), Electrical impedance measurement of plastically deforming halite rocks at 125 °C and 50 MPa, Journal *of Geophysical Research*, *107*, 125-152.

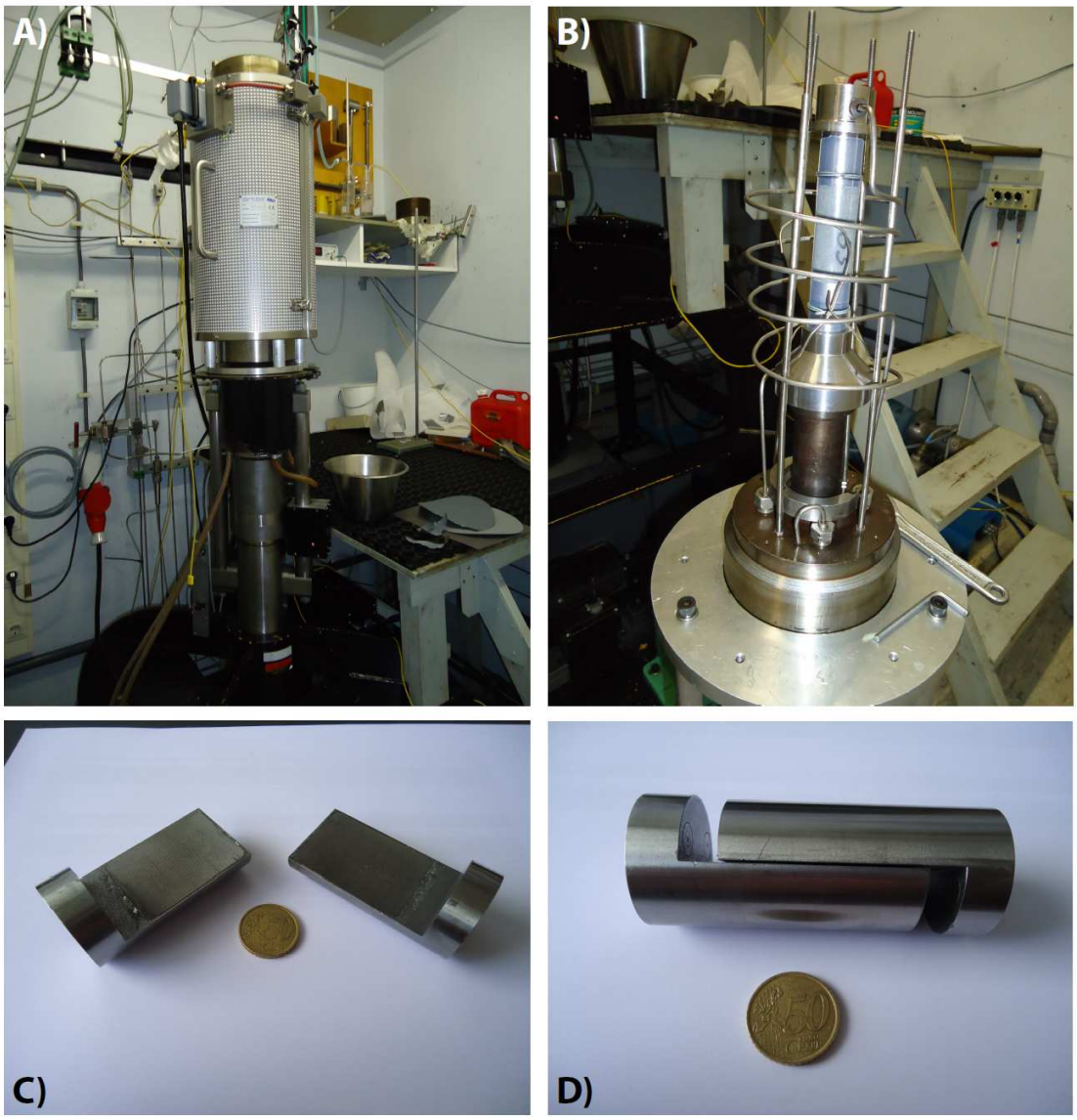

Figure 1 - The Heard Apparatus is a constant confining volume triaxial pressure vessel capable of generating 100 MPa confining pressure at temperatures of up to approximately 250 °C using EPDM and FEP jacketing materials. A) The Heard vessel is surrounded by an external furnace (silver) and is loaded vertically from the bottom of the pressure cell. Temperature is monitored internally, in contact with the experimental sample as well as externally. B) The sample is held in place inside of a heads-piece which is inverted, slid into the top of the Heard vessel, and sealed using o-rings, and a steel on steel cone style connection. Sample shown here is a 25mm diameter rock core, ~60mm in length (UU-Sample I.D.: 55). C) 35mm diameter forcing blocks for "inverted-shear" style direct shear in the Heard apparatus (50 euro cent piece for scale). Both sides of the inverted-shear geometry are fitted with 33 x 47 mm sintered porous steel fluid distribution plates. D) inverted-shear blocks fitted together in experimental configuration, will be placed into the heads-piece in the same configuration as the rock sample in B)

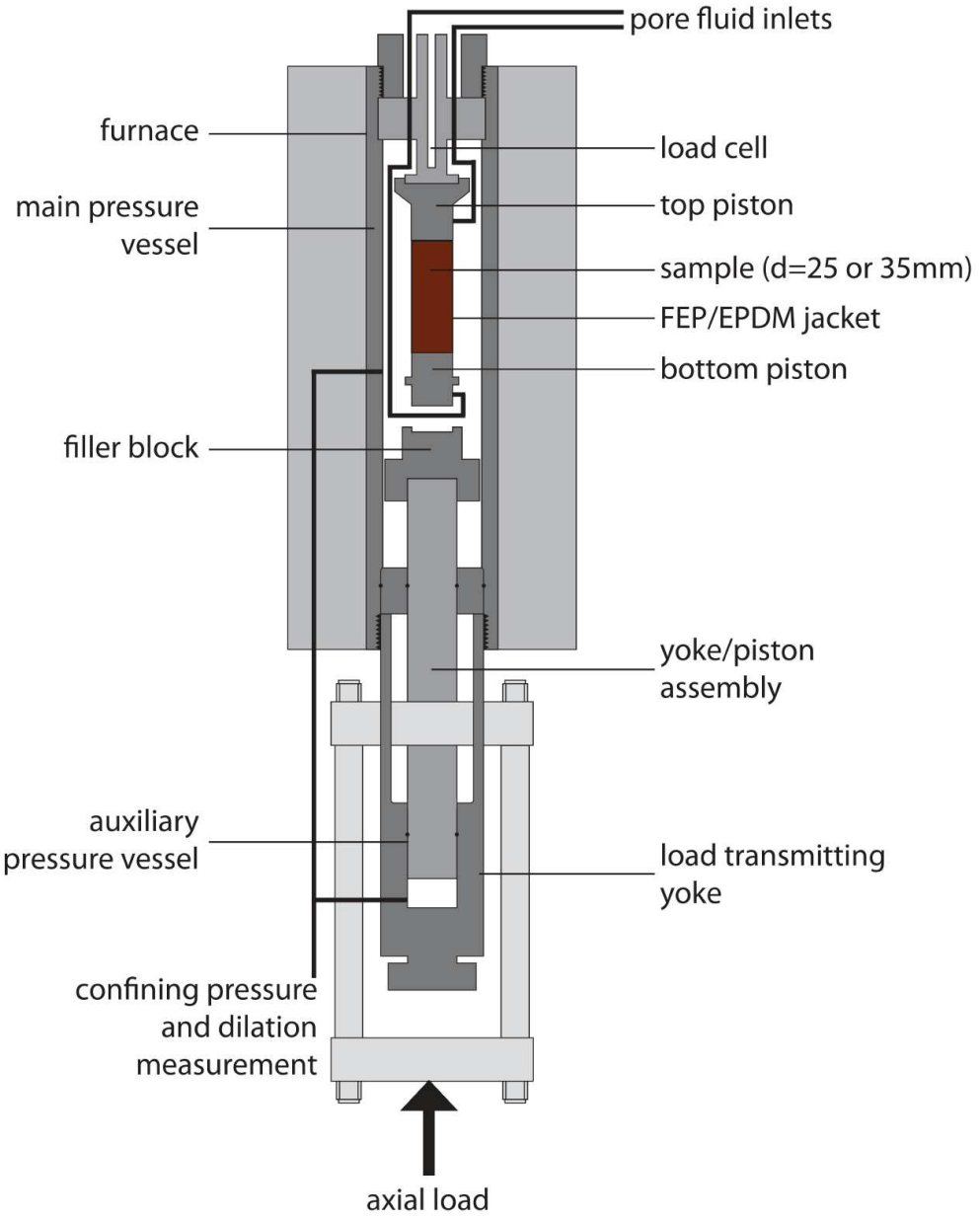

Figure 2 - Schematic of the Heard tri-axial pressure vessel. The experimental sample is fitted between two forcing blocks, labeled here as "top piston" and "bottom piston", and isolated from the confining fluid using either FEP or EPDM rubber jackets. The vessel is first pressurized to approximately 3 MPa, then brought to temperature using the external furnace. As the confining oil undergoes thermal expansion pressure in the vessel is bled off to maintain a value slightly underneath of the intended pressure of the experiment. Once the desired temperature is attained the vessel is brought to experimental pressure, and allowed to equilibrate for approximately 1 hour. When the Heard vessel has reached pressure and temperature equilibrium the sample is loaded axially from underneath of the pressure vessel at constant velocity. A gearbox at the base of the apparatus allows a 1000-fold range of displacement velocity from nearly tectonic plate rate velocities (~0.05 μm/s) up to speeds within the range of earthquake nucleation (~50 μm/s).

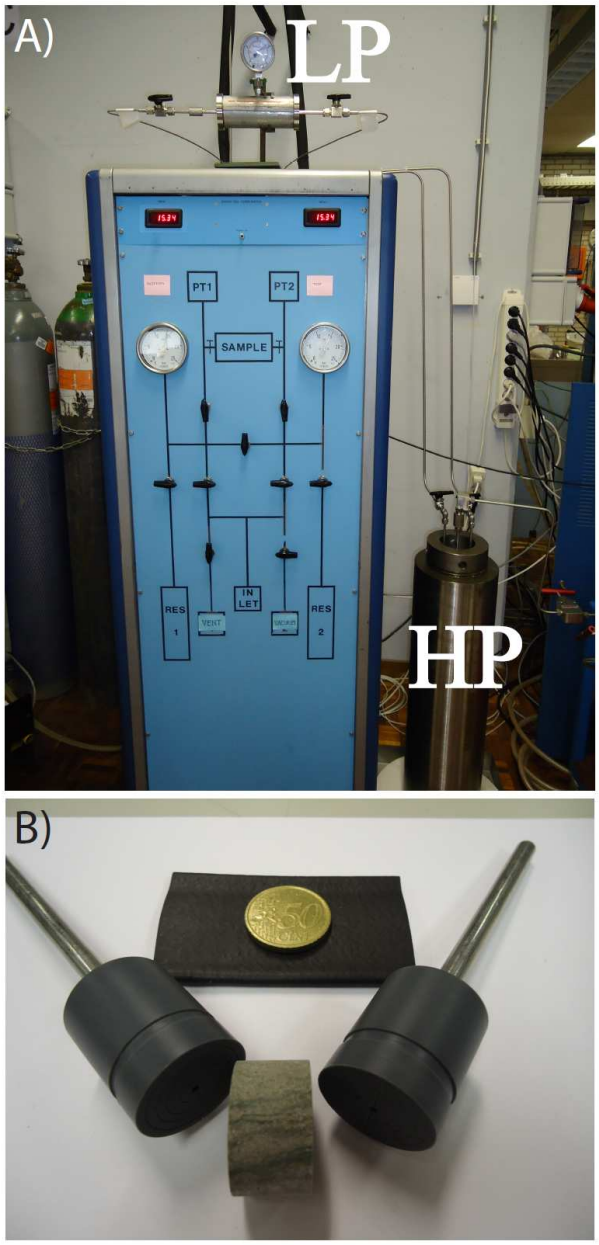

Figure 3 - A) Argon Permeameter (APE) used to make permeability measurements on all samples. Near the top of the APE is a low-pressure cell (labled "LP") used for confining 25 mm diameter cylindrical samples up to ~70 mm in length, at up to 3.5 MPa. On the right hand side of the APE is a recently developed high-pressure cell (labeled "HP") which can be pressurized up to 100 MPa and used to measure the permeability of cap rock and reservoir samples at in-situ pressure conditions. Current procedures limit our ability to measure samples with permeability much lower than ~10^{-19} m^2, but these limitations should be overcome in the near future. B) Sample holders are grooved to allow even distribution of argon gas over the surface of the ends of the sample. Bicyle inner-tube (beneath coin) is used as a jacketing membrane to isolate the sample from the confining pressure, ensuring flow of Argon gas occurs only along the axis of the sample. Sample 14 is shown here also.

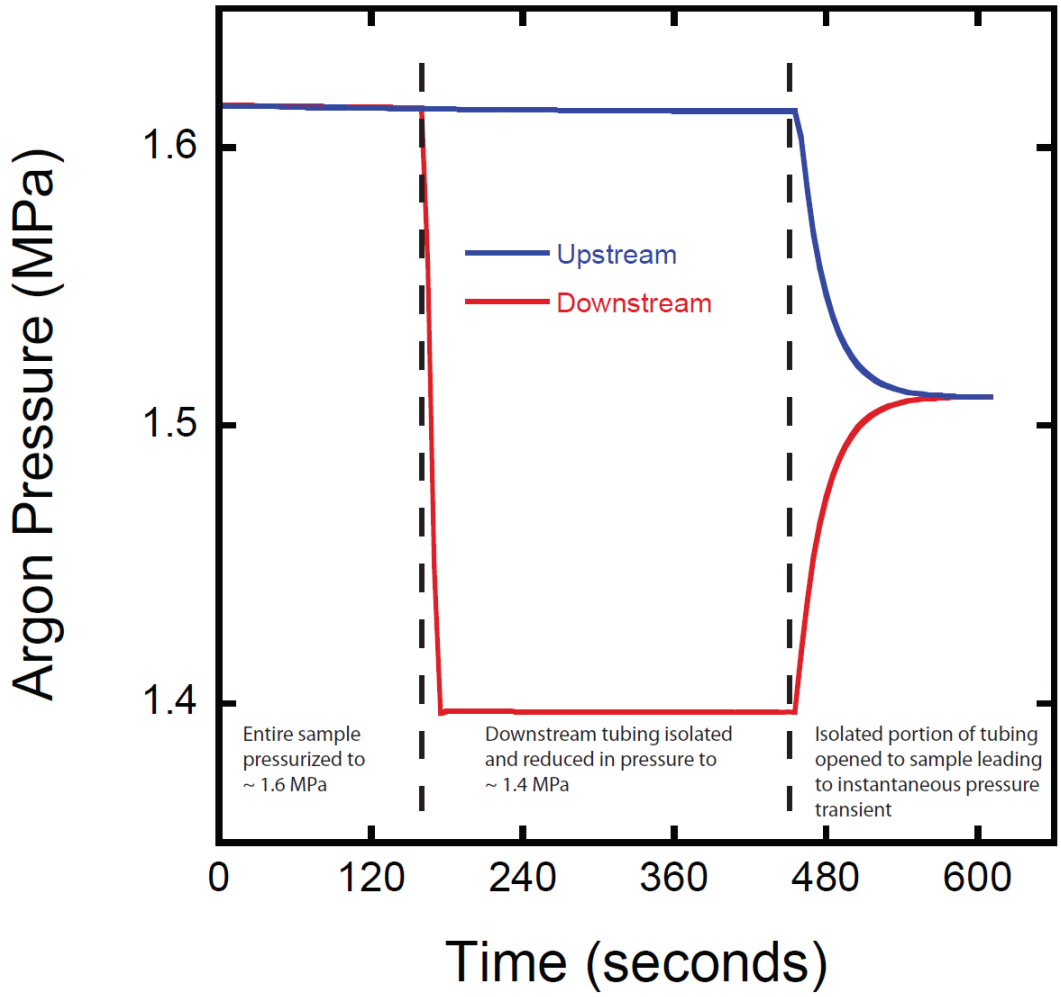

Figure 4 - Results of an Argon-transient-step permeability test in APE LP-vessel. The sample is initially pressurized with approximately 1.6 MPa of Argon fluid pressure. Once the fluid pressure in the sample has equilibrated the downstream side of the APE tubing is isolated from the sample and reduced in pressure to approximately 1.4 MPa. The isolated low-pressure tubing is then opened to the sample, resulting in an instantaneous pressure transient across the sample which decays over time. By measuring the decay of the pressure imbalance across the sample we are able to calculate the permeability.

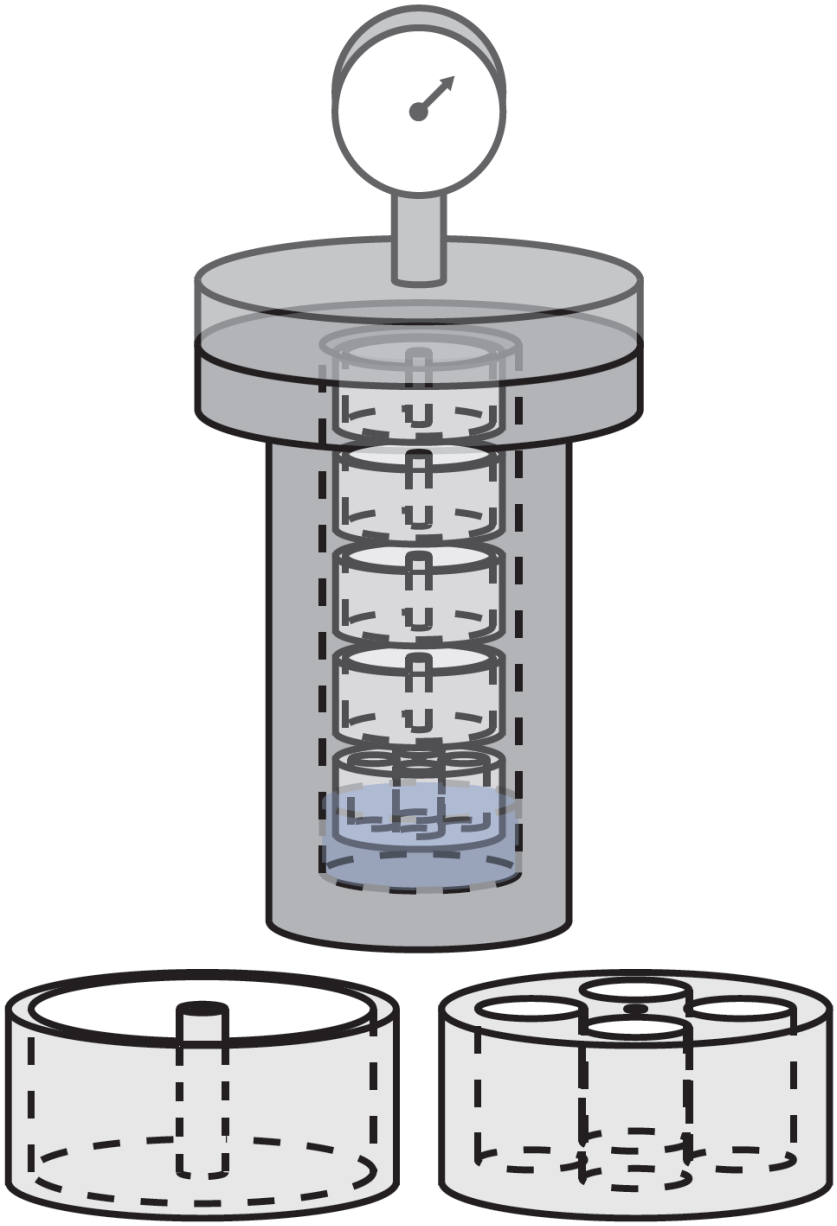

Figure 5 - Schematic diagram of batch autoclave reaction experiments to produce sufficient material for inverted-shear experiments, to measure the long term effect of CO_2 reaction on fault strength and stability. Five 30 mL Teflon pots will be stacked in the autoclave and subjected to 30 MPa CO_2 pressure at ~100 ^{o}C, near in-situ conditions in a sequestration reservoir. We will also include a brine mixture in the base of the autoclave to closely approximate the formation water present in the reservoir (2M NaCl, 0.2M $CaCl_2$, 0.04M $MgCl_2$). Sufficient quantities of sample 12-14 are available for this procedure, and have been powdered to fill four of the Teflon pots. The remaining pot will be used for experiments relevant to WP 3.4.

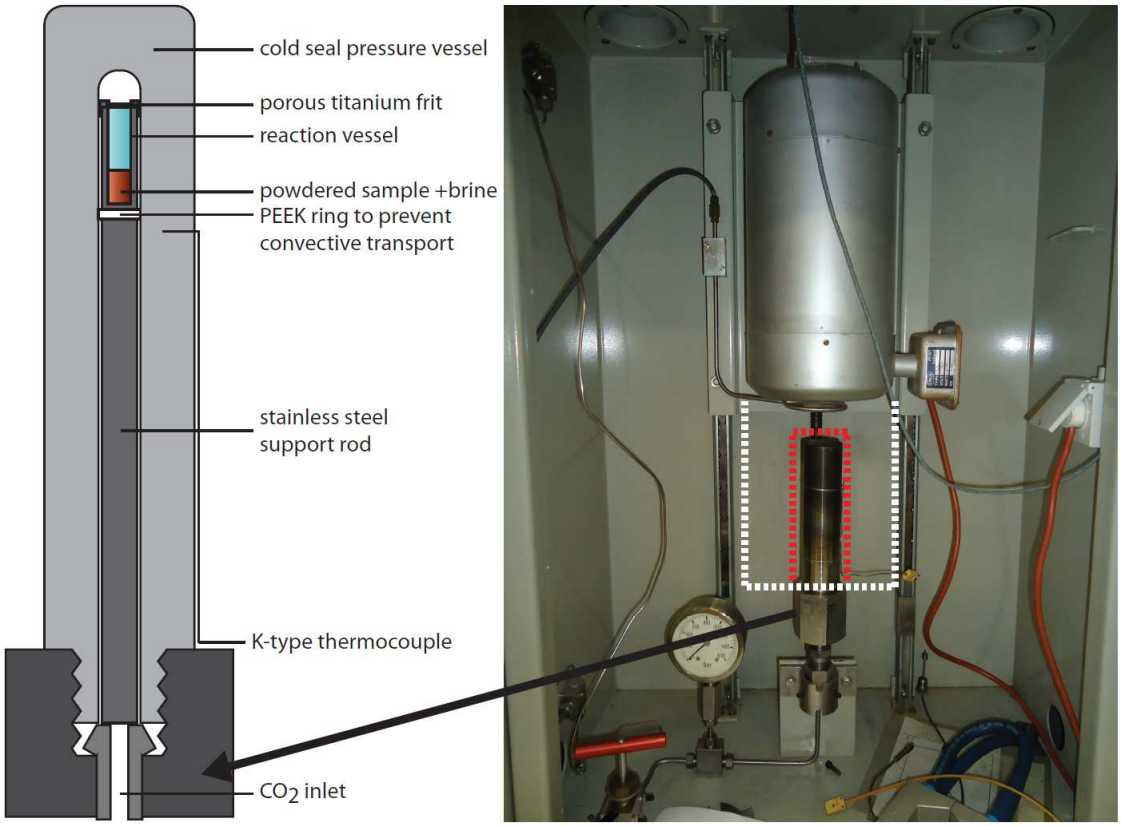

Figure 6 - Cold seal pressure vessel used for reaction of cap rock material. Samples of ~ 0.1 g are heated and pressurized with CO_2 to in-situ conditions (35 MPa, 115 °C). The duration of experiments can be systematically controlled in order to determine at what point during CO_2 sequestration mineral assemblages may form. The photograph shows the cold seal pressure vessel in place (outlined in red) before the furnace has been lowered into place over the pressure vessel (outlined in white).

TNO-RIJSWIJK PRINS MAURITS LABORATORY – EXPERIMENTAL METHODS

Batch experiments on reaction between caprock and CO_2-rich brine:

Background, framework & status

In contrast to hydrocarbons, CO_2-rich fluids are chemically active at reservoir conditions. Storage of CO_2 in depleted gas reservoirs or aquifers may result in chemical reactions affecting reservoir, caprock or faults. If chemical reactions take place at sufficient high reaction rates, it will change the transport and mechanical properties of caprock and may affect the long-term integrity of top seals. Therefore, in order to assess leakage risks of CO_2 through top seals at storage sites, the rate and impact of reactions between CO_2-rich fluids and caprock needs to be known. Static experiments on caprocks in contact with CO_2-rich fluids at reservoir conditions can be used to quantify reaction rates and study the impact of reactions on caprock samples.

This section describes the development of a laboratory facility at the Prins Maurits Laboratory of TNO in Rijswijk. The facility is developed to perform static reaction experiments between CO_2-rich brine and caprock as well as reservoir rock and wellbore cement at downhole/reservoir conditions. Development of the facility is therefore carried out within the framework of WP3.2 (Reservoir Behavior), WP3.3 (Caprock and Fault Integrity) and WP3.4 (Well Integrity).

An initial test facility was developed and used to carry out reaction experiments between CO_2-rich brine and wellbore cement (Figure 1). These experiments showed that some improvements to the setup were needed to reduce the brine to sample ratio and shield samples from the CO_2-rich brine acting as the pressure medium. Improvements to the setup and initial experiments on caprock samples are planned for year 2 of CATO-2.

Figure 1 Left: Pressure vessel and Teflon reservoir containing 3 small cement samples, brine and a stirring device. Right: Experimental setup with the heat bath on the left and the vessel on the right, isolated by glass wool. Thermocouples and pressure measurement devices are placed on the cover of the pressure vessel and attached to a computer to monitor pressure and temperature of the brine and the supercritical CO_2 during the experiments.

Outlook:

An improved experimental setup is being developed which allows experiments with a more realistic brine to cement ratio (Figure 2). The main change to the initial setup is that an additional sample is placed between an upper and a lower stainless steel piston in an EPDM and FEP jacket and positioned next to a sample in the original sample configuration. Within the vessel a sample in the initial configuration can run simultaneous with a sample in the improved configuration in order to compare the two methods and to investigate the effect of the improved facility. A connection between the supercritical CO_2 in the open vessel and the jacketed sample is possible to allow equal CO_2 pressure and vaporized water content in both experimental settings. The connection can also be closed in case a lower pressure is required in the jacketed sample to prevent leakage through the jacket. Experiments will have to show whether it is necessary to open

the connection to prevent drying out of the jacketed sample and whether leakage in the jacketed sample will occur if the connection is opened. Brine samples can be taken during the experiment through the bleeding/sampling tap. The jacketed sample method is similar as used by *Liteanu* [2009] and therefore comparison of experimental results is allowed. The improved setup will be used to perform experiments on representative samples of caprock and brine compositions (planned for year 2 of CATO-2).

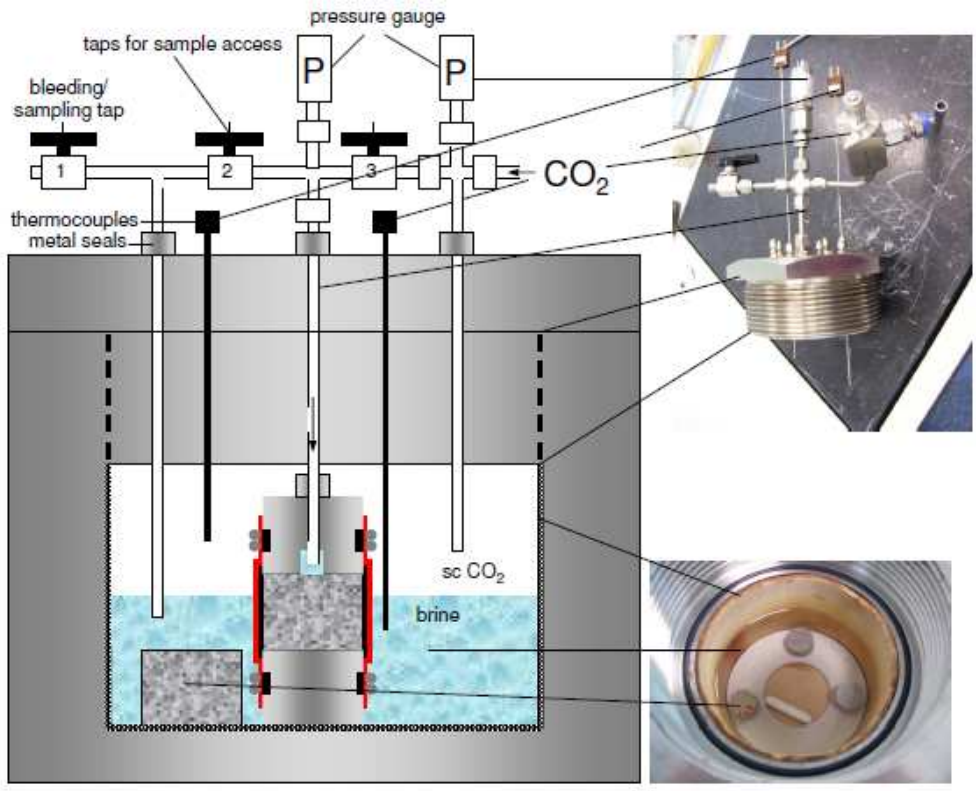

Figure 2 Sketch of improved facility.

References:

Liteanu, E. (2009), Subsurface impact of CO_2, response of carbonate rocks and wellbore cement to supercritical CO_2 injection and long-term storage. PhD thesis ISBN/EAN 978-90-5744-171-4

THE LABORATORY OF GEOTECHNOLOGY AT DELFT UNIVERSITY OF TECHNOLOGY – EXPERIMENTAL METHODS:

Cap rock experiments, rock mechanical property determination from laboratory experiments: translation of laboratory stress and temperature parameters to in-situ values.

CATO-2A: WP3.3, D04 and D09.
Laboratory facilities for transport and mechanical properties determination

K-H.A.A. Wolf

Delft University of Technology, Dept. of Geotechnology, POB 5028, 2600 GA Delft
Stevinweg 1, Room 3.01, 2628 CN, Delft The Netherlands, k.h.a.a.wolf@tudelft.nl

Abstract

CATO-2A: WP3.3,D04 and D09.
Laboratory facilities for transport and mechanical properties determination

The laboratory of Geotechnology at Delft University of Technology owns various types of experimental high P,T equipment. Several consist of pressure vessels which can hold large cylindrical cores, among others fractured rock and coal. Besides determination of the stress-strain behaviour, it is possible to recognize phenomena of rock-fluid interaction and to calculate associated mass balance issues. The annular pressure can be established by either nitrogen or oil pressure upon a rubber sleeve. However, CO_2 has the ability to react with or permeate through the sleeve. In addition, the annular oil can absorb CO_2. For this reason we propose to use lead foil as a barrier between the sample and sleeve. The foil has a temperature and pressure dependent creep behaviour, which has to be compensated when calculating the actual experimental stress on the sample. This actual experimental stress is needed, when the experimental results on fluid/gas migration under in-situ conditions are included in models. In this report we explain a method to be used, to calculate this stress composition. It is based on a series of high T,P of experiments in which fractured rock has been compacted in a copper tube at temperatures up to 1300 K. The major part of the procedure has been described for lead foil. However, a part of the thermo-mechanical data for lead have to be gathered. For these parts the analogue with copper has been inserted.

K-H Wolf

Introduction

The interactions in the system caprock-frac-CO_2-H_2O can be monitored on phenomena such as (fracture) compaction, dissolution, (re-)mineralization and permittivity. At Delft University, pressure vessels can obtain cylindrical cores up to about 2000 cc in which the mentioned results can be acquired. To determine the actual stress on cap rock samples during experimental compressions, the effects of the rubber sleeve and lead foil have to be considered:

- The rubber sleeve acts as an elastical cylinder, which compacts and get stiffer

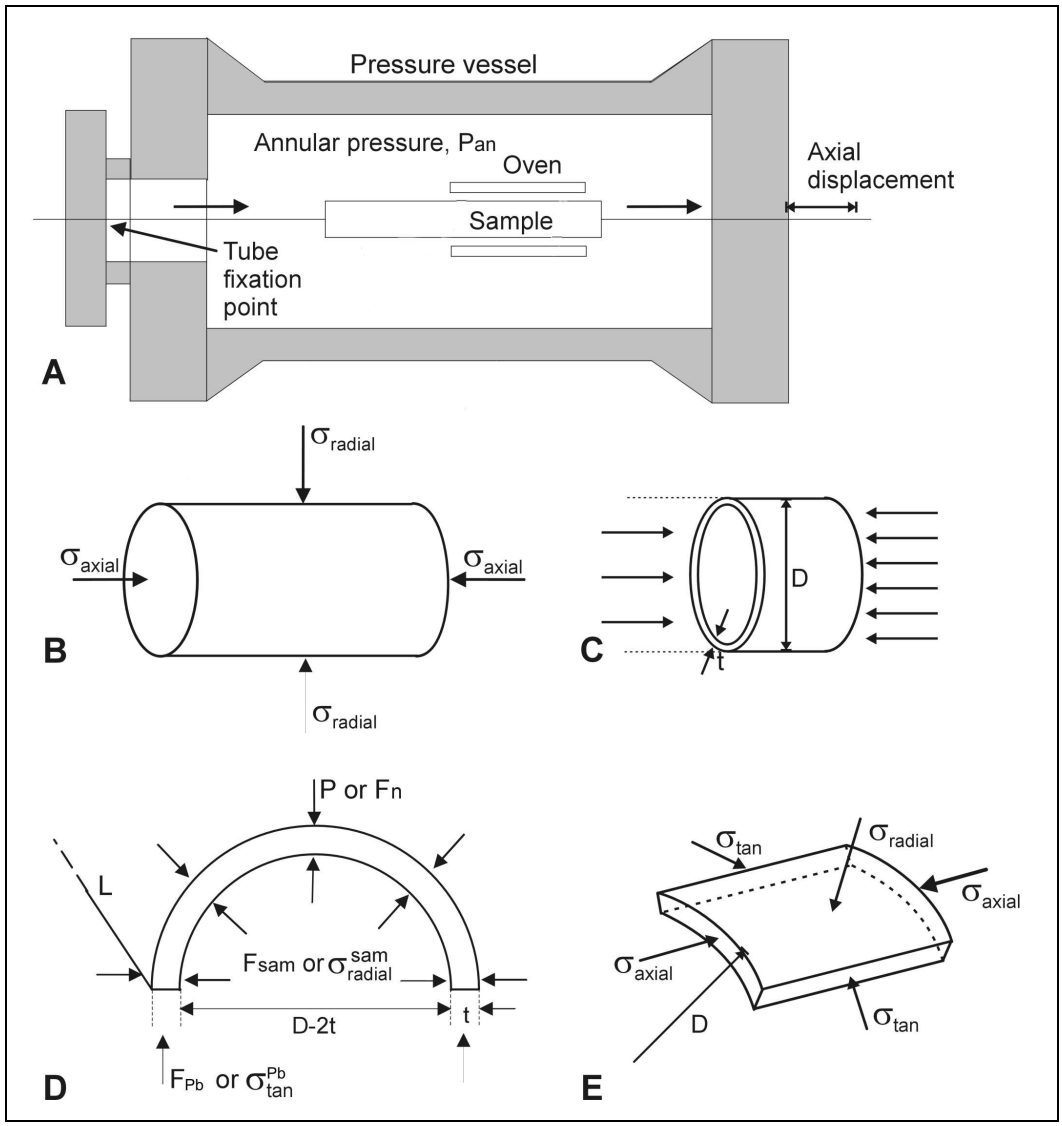

Figure 1. *A, B: The pressure vessel and oil- or nitrogen annular pressure (P) situation of the sample. C: Forces in the axial direction on the sleeve and lead foil. D: Forces in the radial direction on the lead tube. E: Stresses explained on a part of the thin-walled tube.*

with increasing isotropic annular gas pressures in both radial and axial direction (figure 1). We consider this stress absorption negligible. However, when in contact with CO_2 it may adsorb CO_2 or act as a permeable medium towards the annular space.

To optimize the conditions for mass balance calculations and to avoid mixture of sample CO_2 fluids and gases with the annular oil/gas, 0.2 – 1.0 mm thick lead foil is used.

- Lead is soft, malleable and easy to deform, causing fatigue cracking and creep (Table 1). It has a high coefficient of thermal expansion and melts at ca. 327 ºC. The lead layered foil acts as a stress absorber with a temperature dependent plastic behavior. Furthermore, the nature of the deformation depends on the annular pressure and the temperature from the outside and the strength of the sample and pore pressure at the inside; both elastic and visco-elastic behavior is expected.

Table 1: Properties for pure lead		
Density	1.13E+04	kg/m^3
Elastic modulus	13.8	GPa
Poisson's ratio	0.42	
The tensile strength (pure lead, T-dependent)	12-17	MPa
Creep occurs in lead (99.99% purity) at stresses as low as 0.7 MPa (though by a very small amount, elongation of 0.06% after 500 days at 30°C; double the stress produced a 2% extension in the same period (Blasket and Boxall, 1990)). Extrapolation from other tests shows that, under normal conditions, no appreciable creep will be expected at stresses below 1.72 MPa (or if in compression, 2.75 MPa) for 99.9% pure lead (LDA technical notes 1992).		
Heat capacity	130	J/kg*°C
Thermal Conductivity	37.04	W/m*°C
Thermal expansion coefficient	52.74	µm/m*°C

Hence, it is important to define the amount of stress that is absorbed by the lead foil. Based on a previous study on high-T behavior of copper sleeves by Wolf (2006), this study proposes a method to be used for the CATO-2 cap rock compaction and flow experiments.

Determination of Forces and Stresses on the Lead Foil

Balance of Forces for a Thin Walled Foil in the Axial and Radial Direction.

To determine the behaviour of the lead foil at the temperatures and pressures of the compaction experiments, the stresses in the lead are associated to its yield stresses. The wall thickness (*t*) of the lead foil, with an outer diameter (D) and inner diameter of respectively 70 mm and 68 mm, is considered to be thin (t<<D).

The force (F_1) in the axial direction is the gas pressure (P) on the sample and axial lead surface. On the opposite side, the sample exercises a counter force F_2:

$$F_1 = P\frac{\pi}{4}D^2 \qquad \text{eq. 1}$$

$$F_2 = F_{tube} + F_{sample} = \sigma_{ax}^{Cu}\pi\frac{\pi}{4}\left(D^2 - \left(D-2t\right)^2\right) + \sigma_{ax}^{sam}\frac{\pi}{4}\left(D-2t\right)^2 \qquad \text{eq. 2}$$

Since $F_1 = F_2$,

$$P\frac{\pi}{4}D^2 = \sigma_{ax}^{Pb}\pi\frac{\pi}{4}\left(D^2 - \left(D-2t\right)^2\right) + \sigma_{ax}^{sam}\frac{\pi}{4}\left(D-2t\right)^2, \qquad \text{eq. 3}$$

where the gas pressure P is defined as:

$$P = \sigma_{ax}^{Pb}\frac{4t}{D} + \sigma_{ax}^{sam}\left(1-\frac{4t}{D}\right) \qquad \text{eq. 4}$$

Note: Since t<<D, the second order part in eq. A.4 is negligible.

The balance of force (Figure 1.C) in the radial direction is a summation of the gas pressure or normal force (F_n), counter force of the sample (F_{sam} or σ_{rad}^{sam}) and tangential stress in the foil wall (F_{Pb} or $\sigma_{\tan}^{Pb}$):

$$F_N - F_{sam} = PLD - \sigma_{rad}^{sam}L\left(D-2t\right) \qquad \text{eq. 5}$$

$$F_{Pb} = \sigma_{\tan}^{Pb}2tL \qquad \text{eq. 6}$$

L is the length of the foil. Since the tangential stress in the "foil wall" is the summation of the sample stress and normal stress, $F_N - F_{sam} = F_{Pb}$, the pressure on the foil is rewritten as:

$$P = \sigma_{\tan}^{Pb}\frac{2t}{D} + \sigma_{rad}^{sam}\left(1-\frac{2t}{D}\right) \qquad \text{eq. 7}$$

Linear-elastic Behaviour of the Lead Foil Sleeve.

For the lower temperatures lead is expected to behave elastic (E-modulus $1.38*10^{10}$ Pa) and can be calculated. The annular pressure affects an equal radial stress in the foil wall. Hence, the radial and tangential stresses ($\sigma_{rad}^{Pb}, \sigma_{\tan}^{Pb}$) in the foil, as visualized in figure A.1.E, can be expressed as:

$$P = \sigma_{rad}^{Pb} \quad \text{and} \quad \sigma_{\tan}^{Pb} \approx P\frac{D}{2t} \qquad \text{eq. 8, 9}$$

Here the tangential stress is obtained from eq. 7, ignoring the low sample stress (σ_{rad}^{sam}). Now the relationships between the tangential and axial stress, between the radial and axial stress (using eq. 4), are expressed as:

$$\sigma_{\tan}^{Pb} \approx \sigma_{rad}^{Pb}\frac{D}{2t} \qquad \text{eq. 10}$$

$$\sigma_{rad}^{Pb} \approx \sigma_{ax}^{Pb} \frac{4t}{D} \qquad \text{eq. 11}$$

$$\sigma_{ax}^{Pb} \approx \frac{1}{2}\sigma_{\tan}^{Pb} \qquad \text{eq. 12}$$

Since the wall thickness (max 1 mm) is much smaller than the tube diameter (ca. 70 mm), the radial and axial stresses are smaller than the tangential stress:

t<<D $\Rightarrow$ $\sigma_{rad}^{Pb} << \sigma_{\tan}^{Pb}$, $\sigma_{rad}^{Pb} < \sigma_{ax}^{Pb}$ and $\sigma_{\tan}^{Pb} \approx 2\sigma_{ax}^{Pb}$

When considering elastic behaviour with linear deformation, which means that stress and strain are linearly associated Hooke's law can be applied. In case of a hydrostatic stress, the translation of the stresses in the thin-walled foil to strain values in the axial direction, gives:

$$\varepsilon_{ax}^{Pb} = \frac{\sigma_{ax}^{Pb}}{E} - \frac{\nu}{E}\sigma_{\tan}^{Pb} - \frac{\nu}{E}\sigma_{rad}^{Pb} = \sigma_{ax}^{Pb}\left(\frac{1-2\nu}{E}\right), \qquad \text{eq. 13}$$

Translated into K_b^{Cu}, the bulk modulus term for lead, using $K_b^{Pb} = \frac{E}{3(1-2\nu)}$, gives the stress-strain relationship :

$$\sigma_{ax}^{Pb} = K_b^{Pb} 3\varepsilon_{ax}^{Pb} \qquad \text{eq. 14}$$

Returning to the foil-sample relationship with isotropic stress, and isotropic deformation of the sample, or $\varepsilon_{11}^{sam} = \varepsilon_{22}^{sam} = \varepsilon_{33}^{sam}$, the gas pressure can be associated to the bulk moduli and axial strain for both the sample and foil. Using the equations 4 and 14 gives the pressure on the bulk lead + sample of:

$$P = 3K_b^{Pb}\varepsilon_{ax}^{Pb}\frac{4t}{D} + 3K_b^{sam}\varepsilon_{ax}^{sam}\left(1-\frac{4t}{D}\right) \qquad \text{eq. 15}$$

Since the axial strain in the lead (ε_{ax}^{Pb}) and sample (ε_{ax}^{sam}) are the same,

$$P = 3\varepsilon_{ax}^{Pb,sam}\left(K_b^{Pb}\left(\frac{4t}{D}\right) + K_b^{sam}\left(1-\frac{4t}{D}\right)\right) \qquad \text{eq. 16}$$

The bulk modulus of lead and sample (K_b^{tot}) is associated to the hydrostatic stress (ΔP) and associated isotropic strain ($\Delta\varepsilon_V$); $K_b^{tot} = \frac{\Delta P}{\Delta\varepsilon_V}$ or $K_b^{tot} = \frac{\Delta P}{\Delta(3\varepsilon_{ax})}$.

Substitution gives for the total bulk modulus:

$$K_b^{tot} = K_b^{Pb}\left(\frac{4t}{D}\right) + K_b^{sam}\left(1-\frac{4t}{D}\right) \qquad \text{eq. 17}$$

Bulk rock samples with wide open fractures or fractured coal samples, may initially give the same results as tight packed grain aggregates, when compacted. Neuman (1998) shows in uni-axial compression experiments on thermally treated grain aggregates, that bulk moduli of the sample are negligible or comparable to those of the linear elastically deforming foil. So the minimum total bulk modulus is:

$K_b^{tot} > K_b^{Pb}\left(\frac{4t}{D}\right)$, based on a $K_b^{Pb} \approx 14$ GPa at room conditions.

Visco-Elastic Behaviour of a Lead Foil Sleeve.

The visco-elastic behaviour of a thin lead foil wall has not been calculated, since no relevant data have been assembled. Hence we discuss in this section *an analogue* for a copper tube at higher temperatures. Studies by DMG (1985), Dahlman (1988) and McQueen (1991) stated that, at elevated temperatures, the yield stress (σ_y) of copper is a function of temperature (*T*) and deformation rate ($\dot{\varepsilon}$), or $\sigma_y = f\left(T, \dot{\varepsilon}\right)$. Figure 2 shows that, up to a certain stress, the stress-strain curve is linear with elastic deformation. Above this stress, the yield stress (σ_y), the elastic deformation turns into permanent plastic deformation.

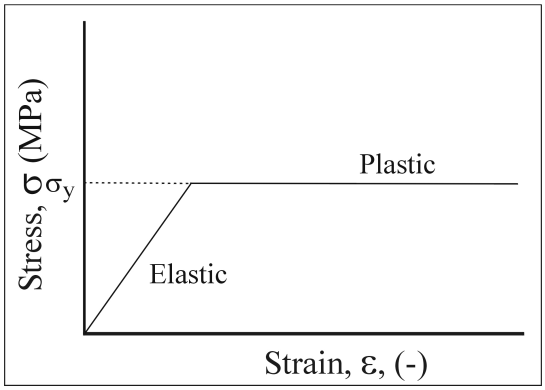

***Figure 2**. Stress – strain curve for perfect visco-elastic behaviour.*

In a stress strain curve for ductile creep these phases are detectable but less clear. The transition from elastic to plastic behaviour is not sudden but gradually. The higher the temperature, the lower the yield stresses. The higher the strain rate, the higher the yield stresses. In general, if the temperature is higher than half the melting temperature creep can be described by a power law function (Kirby, 1984).

DMG (1985) presented a wide range of uni-axial experimental results on high grade copper (Cu > 99.9%). From 500ºC – 900ºC and at strain rates varying from ~10^{-3} s^{-1} to 93 s^{-1}, a wide range of flow stresses, varying from 28 MPa to 200 MPa, were measured. The meagrely described experimental results are difficult to compare, since copper samples with different grain sizes, textures and compositions are used. Nevertheless, flow stress increases with increasing strain rates and decreasing temperatures. At low strain rates (< 10^{-1} s^{-1}), the flow stress is in between about 20 MPa and 50 MPa. McQueen (1991) confirms the behaviour in his compendium on copper/lead alloy creep behaviour. At temperature above circa 400℃ and deformation rates below 10^{-3}, or low stresses, the copper deformation follows the conventional power law creep law and behaves as an elasto-plastic medium:

$$\dot{\varepsilon} = A\sigma^n e^{-E_a/RT}, \qquad \text{eq. 18}$$

where: $\dot{\varepsilon}$ is the creep rate (s^{-1}), *A*; the creep scaling constant (($Pa^{-n}.s^{-1}$), σ; applied stress (MPa), *n*; creep stress exponent (-), E_a; the activation energy (kJ/mol), *R*; gas constant of 8.3144 j/mole.K and *T*; the temperature (K). The compendium copper creep of McQueen (1991), explains that the activation energies (*Q*) for the different copper types vary from 227 kJ/mol to 340 kJ/mol. Dahlman (1988) referred to lower values of 197 kJ/mol to 234 kJ/mol, obtained by Ilschner (1973). In Dahlman's study on creep behaviour of electrolytic copper at the end of its thermal solid range, 850ºC – 1050ºC, it is also stated that the stress strain behaviour at high temperatures follows the rules for power law creep. Based on equation 18, conversion to a logarithmic linear relationship, the tension exponent, activation energy and scaling constant are derived:

$$\ln\dot{\varepsilon} = \ln A + n\ln\sigma - \frac{E_a}{RT} \qquad \text{q. 19}$$

The following outcomes can be applied to the interpretation of copper behaviour in high temperature compaction experiments to an annular stress of 10 MPa:

- It is observed from the log strain rate – log stress graphical presentation that, for the thermal range of 873 K to 1323 K, the tension exponent (*n*) has an average of 4.35 ± 0.2. For the experiments *n* is considered to be constant; *n* = 4.35.
- It is observed from log strain rate – inverse temperature that, for constant stresses, the activation energy (*E*) is hardly varying; $2.84*10^5 \pm 0.15*10^5$ J. For the stress range of interest, *E* is considered to be constant, $E = 2.84*10^5$J.
- From both, graphical presentations it is observed that A is stress dependent. Within the working area up to 10 MPa, A varies from $4.67*10^3$ - $61.66*10^3$.

The values of table 2 are used for corrections on copper stress data, to correct strain rates at specified temperatures. If the K_b of the sample is considered to be negligible, then the stresses in the lead foil will be higher than the yield stresses belonging to the conditions. Hence, the theory for plasticity interprets the stress-strain behaviour of the sample.

NOTE: For lead foil we propose to follow the same way of thinking as described in the following section, based on creep of copper.

Table 2. *Copper data, derived with the use of experimental results of Dahlman (1988)*

Logσ *LogMPa*	*σ* MPa	*E* J/mole*10^5	*A* 1/(Pa^n.s) *10^3
0	1	2.96	61.66
0.4	2.51	2.98	57.54
0.6	4	2.91	38.02
0.8	6	2.81	11.22
1	10	2.67	4.68
Additional parameters			
K_b^{Cu} GPa	$\overline{n}$ (-)	$\overline{E}$ J/mole*10^5	
140	4.35	$2.84*10^5$	

Determination of Forces and Stresses in the Sample

Stresses Acting on the Sample

The equations 4 and 7 show the relationship between the radial and axial stresses on the sample, the stresses on the lead foil and the annular gas pressure. For the sample, the relationships can be rewritten to an axial and radial relationship:

$$\sigma_{ax}^{sam} = \frac{P - \sigma_{ax}^{Pb}\frac{4t}{D}}{\left(1 - \frac{4t}{D}\right)} \qquad \text{eq. 20}$$

and,

$$\sigma_{rad}^{sam} = \frac{P - \sigma_{\tan}^{Pb}\frac{2t}{D}}{\left(1-\frac{2t}{D}\right)} \qquad \text{eq. 21}$$

The average hydrostatic stress on the sample is:

$$\sigma_{av}^{sam} = \frac{1}{3}\sigma_{ax}^{sam} + \frac{2}{3}\sigma_{rad}^{sam} \qquad \text{eq. 22}$$

As discussed in the previous section, the maximum axial and tangential stress in the lead foil are determined by the yield stress of lead, or, $\sigma_{ax}^{Pb} = \sigma_{\tan}^{Pb} = \sigma_{y}^{Pb}$. Hence, the true average hydrostatic stress above the yield stress of lead is derived by merging eq. 20 and 21 in eq. 22, will be:

$$\sigma_{av}^{sam} \approx \frac{P\left(1-\frac{10t}{3D}\right) - \sigma_{y}^{Pb}\left(\frac{8t}{3D}\right)}{\left(1-\frac{6t}{D}\right)} \qquad \text{eq. 23}$$

During compaction the diameter of the foil, *D*, reduces, the wall thickness, *t*, is assumed to remain constant. Note: Since t<<D, the second order parts in eq. 23 are ignored.

Relationship of Stresses on the Sample and the Lead Foil

Since the grain aggregate is assumed to be isotropic, the hydrostatic stress from the foil on the sample (Figure 1.B) will be a combination of equal axial and radial stresses; $\sigma_{ax}^{sam} = \sigma_{rad}^{sam}$.

Consequently the axial and radial strain in the sample also is equal; $\varepsilon_{ax}^{sam} = \varepsilon_{rad}^{sam}$.

Hence the volumetric deformation factor (ε_v) is defined as:

$$\varepsilon_v = \frac{\Delta V}{V_0} = 3\frac{\Delta L}{L_0} - 3\left(\frac{\Delta L}{L_0}\right)^2 + \left(\frac{\Delta L}{L_0}\right)^3,$$

where the volumetric strain approximates three times the axial strain; $\varepsilon_{V}^{sam} \approx 3\varepsilon_{ax}^{sam}$. Accordingly, using Hooke's law for the linear elastic properties of the sample, then gives:

$$\sigma_{ax}^{sam} = \sigma_{rad}^{sam} = K_b\varepsilon_v, \qquad \text{eq. 24}$$

Translated to the stresses in the lead foil, combining the equations 4, 7 and 24, gives:

$$\sigma_{ax}^{Pb} = \frac{P - K_b\varepsilon_v\left(1-\frac{4t}{D}\right)}{\frac{4t}{D}} \qquad \text{eq.25}$$

and,

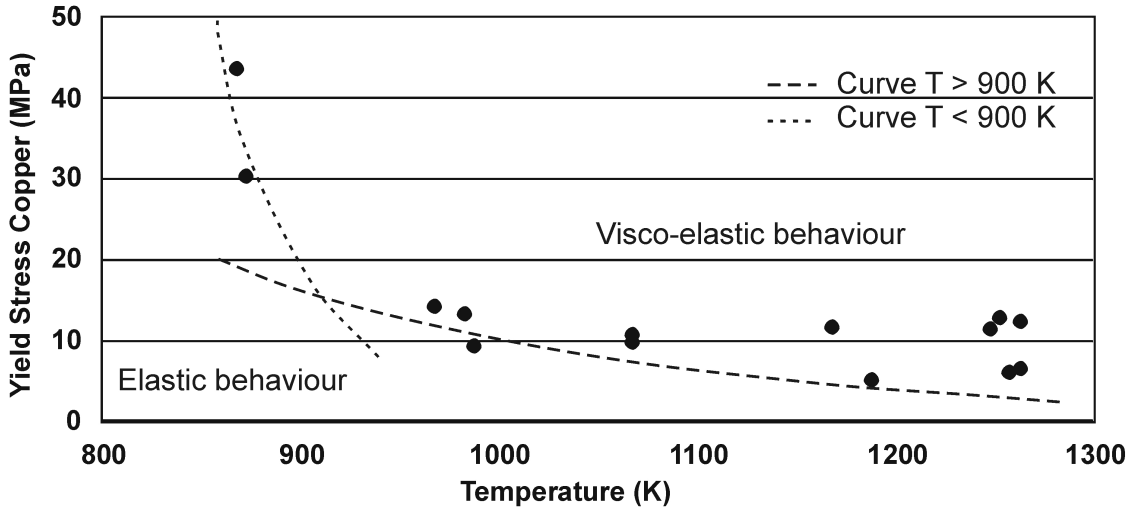

Figure 3: *Example for high-T copper yield stress of a lead tube, based on experiments; T, P, $\dot{\varepsilon}$, and data of Dahlman (1988), McQueen (1991) and Houten (1989).*

$$\sigma_{\tan}^{Pb} = \frac{P - K_b \varepsilon_v \left(1 - \frac{2t}{D}\right)}{\frac{2t}{D}} \qquad \text{eq. 26}$$

When these stresses go beyond the yield stress for lead (σ_y^{Pb}), elasto-plastic behaviour will govern the compaction process. In addition, as demonstrated in equation 22 for the sample, the same relationship is valid for the lead foil:

$$\sigma_{av}^{Pb} = \frac{1}{3}\sigma_{ax}^{Pb} + \frac{2}{3}\sigma_{\tan}^{Pb}. \qquad \text{eq. 27}$$

Figure 3 shows (<u>*as an example the analogue copper*</u>), the calculated yield stress based on experimental conditions of a series of rubble compaction experiments. For an averaged creep stress exponent *n*, *A* is defined as the stress dependent relationship;
$A = 6.81*10^{4}$-$7.03*10e^{3} * P$. The volumetric strain $\dot{\varepsilon}$ is derived from Dahlman, (1988, fig. 43). For T < 900 K; $\sigma_y^{Cu} = 5*10^{113} * T^{-38.074}$, for T > 900 K; $\sigma_y^{Cu} = 1.48*10^{10} * T^{-2.99}$. In the temperature-stress region above the curve the lead behaves visco-elastic, below, i.e. 870 K, elastic behaviour is the driving conduct. When these stresses are lower than the yield stresses for elastic copper, the rigidity of the copper tube or foil minimizes compaction.

Figure 4 shows the temperature build-up, pressure build-up and the elastic and visco-elastic regions during a heating and compaction experiment. To calculate the actual stresses on the sample and foil, the elastic behaviour of the lead foil is to be defined for each high T,P-experiment. *As an example we give the procedure as used with a copper tube compaction experiment:*

- The uncorrected annular pressure increase. The initial pressure build up is usually 0.0033 MPa/s, at a constant temperature.

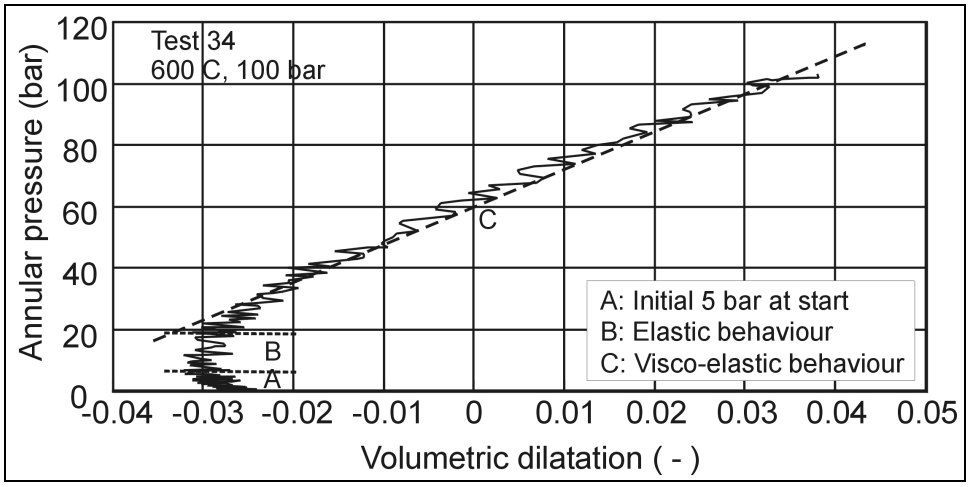

Figure 4. *Compression of the lead tube in test 34. The curve shows the temperature built up (A), pressure built-up (B,C) and associated volumetric dilatation. The pressure and strain give the bulk modulus of the lead tube filled with grain aggregate at a specific temperature.*

- The volumetric strain of the sample and the lead foil ($\dot{\varepsilon}$).
- The associated bulk modulus of the sample and the copper tube (K_B), using eq. 19.
- The foil wall thickness (t), which is considered to be constant.
- The diameter (D), which is associated to the corrected axial displacement, using the same strain values.

Knowing these values, the axial stress (σ_{ax}^{Cu}), tangential stress ($\sigma_{\tan}^{Cu}$), and average stress (σ_{av}^{Cu}) on the copper tube (in our case the lead foil) are derived, using respectively eq. 25, eq. 26. and eq. 27.

If the stresses in the lead foil are known, it is possible to calculate the isotropic stresses on the sample. The axial stress (σ_{ax}^{sam}), radial stress (σ_{rad}^{sam}) and average stress (σ_{av}^{sam}) on the sample are calculated with, respectively, eq. 20, eq. 21 and eq. 23. As mentioned previously, low temperatures and low annular stress results are less credible. The average stresses on the sample will come down to zero. This is in agreement with the experimental results.

Literature:

Dahlman, P., 1988. Zug- Kriech- und relaxationsverhalten von Kupfer bei Temperaturen dicht unterhalb des Schmelzpunktes. PhD-thesis RWTH-Aachen Germany. 60 pages.

DGM, 1985. Atlas der Warmformgebungs-eigenschaften von Nichteisenmetallen. Band 2, Kupferwerkstoffe. Deutsche geselschaft fur Metallkunde, ISBN 3-88355-001-9, 40 pages.

Houten, van, 1989. Technische specificaties voor metalen en legeringen; SE-Cu and SF-Cu. Metaalmaatschappij van Houten BV, - Ridderkerk. 142 pages.

Ilschner, B., 1973. Hochtemperatur-plastizität Reine und angewandte Metallkunde in Einzeldarstellungen. Ed. W. Köster, Band 23. Springer Verlag Berlin, Heidelberg, New York.

Kirby, S.H. & J.W. McCormick, 'Inelastic properties of rocks and minerals: strength and rheology', *Handbook of physical properties of rock*, *III*, 1984, p139-280

McQueen, H.J. 1991. *Hot Workability and Thermo-Mechanical Processing of Copper Alloys,* Plenary Adresses, Economics and Applications of Copper, Proc. Copper 91. Pergamon Press, New York, ISBN 0-08-041432-X, p. 281 - 289.

Neuman, B.V., 1997. *An experimental study to relate compaction with the change in flow properties in thermally treated claystones.* TU Delft-MSc.thesis, Novem-report 94/E0767/230110/0403. (R)

Wolf, K-H.A.A. ,2006. "The interaction between underground coal fires and their roof rocks"., PhD-thesis., ISBN-10: 90-9020939-5, ISBN-13: 978-90-9020939-5. 473 pages.